Journal of Materials Chemistry A

ROYAL SOCIETY OF CHEMISTRY

PAPER

View Article Online
View Journal

Cite this: DOI: 10.1039/d5ta10407f

Sustainable conductive ink for printed "greener" supercapacitors

Leire Sanchez-Duenas, *[ac] Chirag Mevada, *[b] Timo Punkari, [b] Estibaliz Gómez, [a] Estibaliz Aranzabe, [a] Matti Mäntysalo [b] and J. L. Vilas-Vilela [c]

The increase in electronic waste highlights the need to develop sustainable, bio-based, and recyclable electronic systems. Printed electronics offer a promising route to reduce material consumption, though the inks used often contain environmentally harmful components. Conductive inks typically comprise functional materials, binders, solvents, and additives, which are not always as sustainable as desired. To address these issues, the development of sustainable ink must focus on using bio-based, biodegradable, and non-toxic materials. While metals such as silver and gold offer high conductivity, they are costly and not sustainable. Alternatives such as carbon materials or conductive polymers are being explored. Biodegradable polymers such as cellulose, chitosan, PLA, and PVA are viable binders, and "greener" solvents such as Cyrene and ethyl lactate could replace harmful solvents. Energy storage applications manufactured by printed electronics could benefit from these sustainable innovations. In particular, the development of greener supercapacitors (SCs, which offer high power density) using green inks in current collectors (CCs) and electrodes is being studied. In this work, the formulation of sustainable conductive inks for CCs in SCs was studied. The proposed inks used natural graphite flakes as functional materials. Two binder matrices were proposed. The first one involved using cellulose nanocrystals dissolved on PEDOT:PSS, and the second one involved using PLA dissolved on Cyrene. The electrical performance and suitability for CCs of printed SCs were evaluated. The PLA binder-matrix was the best option to develop an SC. This ink also provided better electrochemical performance than the commonly used commercial ink. A fully printed SC was manufactured in this work using the developed PLA ink printed onto a PET substrate. The electrodes were printed using YP-80F activated carbon. Cellulose paper was used as the separator. The electrolyte was a biodegradable, reline-based system. The printed SC was compared with the ones manufactured with commercial inks, showing the advantages of using our new formulation.

Received 22nd December 2025
Accepted 2nd March 2026

DOI: 10.1039/d5ta10407f

rsc.li/materials-a

Introduction

Nowadays, due to the increase in electronic demand and obsolescence of computer programs, there has been a growth in electronic waste.[1] At this juncture, the development of new sustainable, bio-based and/or recyclable electronic systems becomes necessary. To ensure the sustainability of electronic systems, different strategies could be followed. These include reducing the quantity of the materials used in fabrication by selecting an appropriate manufacturing method or substituting the materials for more bio-based or biodegradable ones, avoiding those considered harmful for the environment. Printed electronics represent a good manufacturing method to reduce material consumption. This manufacturing method involves the use of inks or pastes, which are not always sustainable, due to the use of harmful or non-recyclable materials.

Developed inks for printed electronics are composed of four main material groups: (1) functional material, which ensures the desired behaviour of the ink; (2) binder or polymeric resin, where the functional material is carried; (3) solvent, to improve dispersion of the functional material; (4) additive, which helps to improve certain properties of the inks, such as adhesion or stability.[2,3] Focusing on electrically conductive inks, the commonly used functional materials are metallic materials such as gold or silver, which entail high use of precious materials.[4] These metals are used due to their electrical conductivity, with up to 10^7 S m^{-1} being achieved. Other electrically conductive materials are also used, such as carbon or poly(2,3-dihydrothieno-1,4-dioxin)–poly(styrene sulfonate) (PEDOT:PSS), achieving conductivity values up to 10^5 S m^{-1}.[5] Functional materials are carried on a binder, usually a polymeric resin (such as an epoxy resin), which imparts the mechanical properties to the ink. The solvent used to formulate

[a]Surface Chemistry & Nanotechnologies Unit, Fundación Tekniker, Inaki Goenaga 5, 20600 Eibar, Spain. E-mail: leire.sanchez@tekniker.es
[b]Faculty of Information Technology and Communication Sciences, Tampere University, Tampere, Finland. E-mail: chirag.mevada@tuni.fi
[c]Department of Physical Chemistry, Faculty of Science and Technology, University of the Basque Country, UPV/EHU, Barrio Sarriena s/n, 48940 Leioa, Spain

an ink depends on various factors, such as compatibility with the functional material or binder. Different types of solvents, such as water, ethanol, acetone, *N*-methyl-2-pyrrolidone (NMP), *N*,*N*-dimethylformamide (DMF) or dimethyl sulfoxide (DMSO), could be used. However, many of these solvents (*e.g.*, DMF or NMP) are not environmentally friendly, as they are harmful and have high boiling points.[6]

In this context, the development of sustainable inks to produce "green" electronics is a challenge. To ensure the sustainability of an ink, the final composition of the ink must be considered. Depending on the deposition method, the composition of an ink may vary. Table 1 details the percentage of each of the components of an ink for screen-printed and piezo-jet printing technologies.

An ink should be considered "sustainable" if its compounds are bio-based, if they are considered not harmful for the environment, and/or if the ink is biodegradable.[2] Bio-based compounds are those arising from a renewable or natural source, such as carbon particles produced from plants. However, as noted with bio-based plastics, there is no standard to measure the sustainability of an ink considering its bio-based components.[7] Biodegradability is measured by UNE-EN ISO 14855 rule[8] for plastics in ambient compost or by UNE-EN ISO 14852 (ref. 9) in aqueous media, which could be extended for inks. Some biodegradable polymers can be found in nature or be synthesized. Examples of natural biodegradable polymers are chitosan[10] or cellulose,[11] and examples of synthetic polymers are polylactic acid (PLA)[12] or polyvinyl alcohol (PVA).[13] These polymers need to be considered while developing a sustainable ink for printed electronics. Considering solvents, greener solutions are available to develop conductive inks. For example, dihydrolevoglucosenone (commercial name: Cyrene)[14] is a biodegradable and bio-based solvent developed to substitute for DMF or NMP. Another example is naturally obtained ethyl lactate, which can be used as a substitute for toluene, xylene, or acetone.

Different sustainable inks with carbon as the functional material have been reported. Pan *et al.* developed an ink for screen printing using graphene and Cyrene as the solvent.[15] Najafi *et al.* formulated a screen-printed ink with graphene nanoplates in PLA binder.[16] Brooke *et al.* synthesized a carbon black ink for screen printing using nanocellulose as a binder.[17] Zappi *et al.* developed a screen-printing ink using carbon obtained from lignin and cellulose acetate as a binder.[18] Rocha *et al.* manufactured a water-based graphite ink for biosensing applications.[19]

Printed electronics could be used to develop multiple electronic systems or applications. One of the fields in which printed electronics can be applied is energy storage for developing supercapacitors (SCs). SCs are alternatives to batteries to store energy, which can be made of non-toxic materials.[20]

An SC is an electrochemical component that can provide higher specific power than batteries (which exhibit lower specific energy).[21] SCs can be manufactured by printing methods.

Printed SCs can consist of five types of structure: (1) two current collectors (CCs) printed on a substrate; (2) two porous electrodes printed on top of a CC; (3) an ionically conductive electrolyte which is absorbed by electrodes; (4) a permeable separator, to separate both electrodes; (5) a sealant, to maintain the electrolyte on electrodes. A scheme of printed SC architecture is shown in Fig. 1.

CCs have a strong impact on the overall performance of SCs. Most commercial SCs rely on aluminium CCs.[24,25] They offer good conductivity and strength, but often struggle with weak adhesion, corrosion, and surface degradation. Researchers have tried many ways to improve them, including electrochemical etching, chemical vapor deposition, and laser texturing, which create porous features that help the electrolyte interact better with the metal.[26] Carbon materials opened a new chapter. Carbon nanotubes, graphene, and carbon fibres brought high conductivity, flexibility, and stability, making it easier to support fast movement of electrons and ions.[27] Surface tuning methods such as vapor deposition, electrochemical etching, and plasma treatment further improved the contact between the carbon collector and active layer.[28–30] Polymers and fibre-based papers added even more options, offering impressive mechanical flexibility and very low weight, although they fall short with respect to charge storage and long-term cycling.[31] Each class has helped the field grow, yet each brings its own limitations in performance, stability, or environmental impact.

As SC research moves toward cleaner and more scalable technologies, the need for a different type of CC becomes clear. Fabrication methods such as roll-to-roll printing and additive manufacturing point towards printed electronics as the most practical direction. Recent reviews on printed flexible SCs have highlighted that ink formulation, rheological control, and the development of a printable electrode and CC materials are key factors enabling scalable fabrication of high-performance devices.[32] Those studies emphasize the importance of designing conductive inks that balance printability, electrical

Table 1 Ink composition for screen printed and piezo-jet printing technologies[5]

Material	Screen printing	Piezo-jet printing	Ref.
Functional material	5–70%	10–30%	22 and 23
Polymeric resin/binder	20–50%	5–30%	22 and 23
Solvent	15–65%	60–90%	22 and 23
Additives	<5–10%	<5–10%	22 and 23

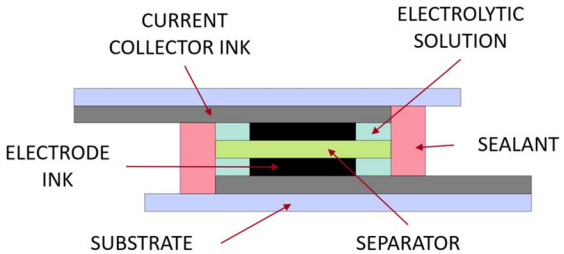

Fig. 1 SC architecture (schematic).

performance, and mechanical flexibility, which directly aligns with the motivation of the present work. Simultaneously, the field of flexible energy storage is shifting towards safer and more environmentally compatible systems. Emerging research on aqueous and proton-based SCs demonstrates the potential of low-toxicity, high-ionic-conductivity electrolytes for sustainable devices.[33]

Within this context, sustainable conductive inks represent a natural progression, enabling printed CCs that can be processed at low temperatures, applied on compostable substrates, and disposed of with reduced environmental burden compared with metal foils or synthetic polymer composites. Sustainable CCs can be synthesized from Earth-abundant, non-toxic materials while providing the conductivity and mechanical integrity required for device operation. Integrating performance, sustainability, and manufacturability makes such materials strong candidates for next-generation environmentally friendly SCs. Recent literature also highlights that wearable and printed SCs depend not only on materials but also on compatible device architectures that ensure flexibility, lightweight design, and scalable processing.[34] Our approach contributes to this direction by combining a printable, bio-based CC with conventional carbon electrodes in a device configuration compatible with flexible energy storage.

Our research team has been using commercially available conductive carbon inks as CCs for SCs research for the past 5 years. We use these inks because they print reliably, offer good sheet resistance of ~14 Ω per square at a 20 μm thickness when cured at 120 °C, and fit our goal of working with materials that have low environmental impact and reasonable biodegradability.[35–44] For comparison, state-of-the-art fully biodegradable printed SCs have been reported to have a sheet resistance of ~23 Ω per square at a much thicker 170 μm CC. Commercial graphite sheets, such as the T68 grade from T-Global Technology, provide excellent conductivity, but they are very fragile and crack readily, which makes them unsuitable for scalable and reliable electrode fabrication.[45] Although these commercial carbon inks have been useful, they are expensive, and their sheet resistance is higher than what is ideal for high-performance SCs. In addition, their exact compositions are proprietary, which makes it difficult to carry out an appropriate life-cycle assessment or evaluate their biodegradation behaviour. This limits our ability to fully understand their environmental impact and restricts further optimization. This motivated us to develop our own formulation that is more affordable, offers lower resistance, and aligns with our focus on sustainable materials.

In this work, we introduced bio-based, PLA binder-based ink formulations that not only lower material costs but also provide better electrochemical performance than the commercial CC inks commonly used in SCs. We demonstrated a nontoxic SC built with materials chosen to support biodegradability and low environmental impact. The device used our PLA binder ink printed on a PET substrate, which served as a reference platform and could be replaced by cellulose diacetate or PLA-based films in future work. The electrodes were made with YP-80F-activated carbon, the separator was cellulose paper, and the electrolyte was a biodegradable reline-based system. To benchmark performance, we compared the devices fabricated with our ink with those made using a commercial high-conductivity carbon ink (LOCTITE EDAG PF 407C E and C) under identical testing conditions. For clarity, this commercial high-conductivity carbon ink is referred to as "commercial highly conductive carbon ink" (HCC ink) throughout this contribution. This comparison allowed us to show the advantages of the new formulation and highlight its potential for sustainable, printed energy storage.

Experimental section

Materials

Natural graphite flakes (99% carbon), Cyrene, PEDOT:PSS water dispersion, chitosan derived from shrimp shells (product 50494), acetic acid, choline chloride, and urea were purchased from Sigma-Aldrich. Porous carbon nanopowder (95% purity, 55–75 nm), produced from plants, was obtained from Nanographi. PLA pellets were purchased from UltiMaker. Activated carbon (YP-80F) derived from coconut shell was sourced from Kuraray Chemicals. Cellulose nanocrystals (CNC) were purchased from Cellulose Laboratory. Milli-Q deionized water (Millipore, Merck) was used for experimental procedures. All chemicals were used directly without additional purification. A 125 μm PET film (Melinex ST506, DuPont Teijin Films) was used as the substrate. A Dynacap GT 0.45/40 cellulose membrane from Glatfelter was used as the separator, and SCs were sealed with 3M 468 MP adhesive.

Synthesis of carbon-conductive ink for CC

Two main composition inks were developed as carbon-conductive inks. Table 2 details the materials used for each of the inks, CNC and PLA inks, which use cellulose nanocrystals and PLA as the binder, respectively. Each of the compositions was prepared following its own method, as described below.

CNC ink preparation

To prepare the CNC ink, natural graphite flakes (NGF) and porous carbon nanopowder (PCN) were added to the solvent (PEDOT:PSS water dispersion). Once the particles had been added, the mixture was stirred using a homogenizer (10 basic ULTRA-TURRAX® of IKA brand). Stirring was done for 5 min at maximum speed (30 000 rpm). After stirring, CNCs were added to the obtained mixture, and it was stirred under identical conditions for an additional 15 min, obtaining the final composition of the CNC ink. Fig. 2 is a scheme of the preparation of the CNC ink. Three formulations were prepared using the described method.

The formulations of CNC-based inks are shown in Table 3. The composition of each ink is described in terms of the weight ratio between functional materials and binder, as well as the weight relationship between the binder (PEDOT:PSS) and solvent.

Table 2 Material composition of the developed inks

Material	CNC ink	PLA ink
Functional material	Natural graphite flakes Porous carbon nanopowder	Natural graphite flakes Porous carbon nanopowder
Binder	Cellulose nanocrystals	PLA
Solvent	PEDOT:PSS water dispersion	Cyrene

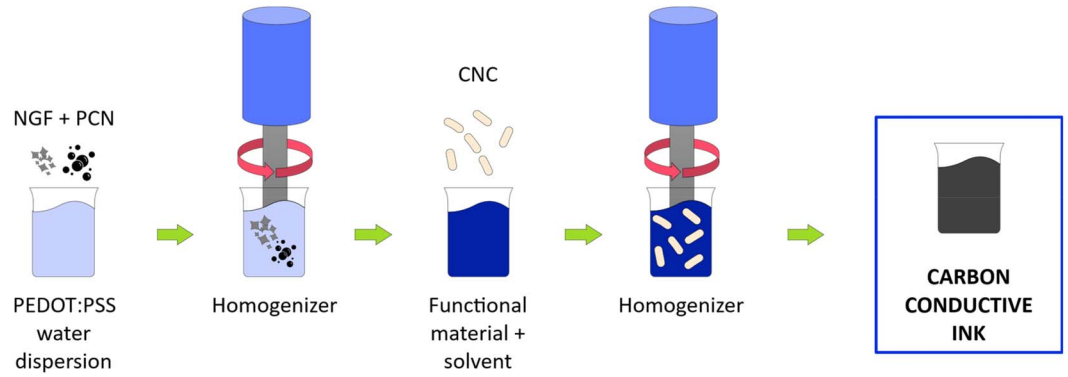

Fig. 2 Preparation of CNC ink.

Table 3 Formulations of CNC-based inks

	Functional material : binder (wt%)		
Name	PCN : CNC	NGF : CNC	Binder : solvent (wt%)
CNC_1	40% PCN : 40% CNC	20% NGF : 40% CNC	5% CNC : 95% PEDOT:PSS
CNC_2	60% PCN : 5% CNC	35% NGF : 5% CNC	1% CNC : 99% PEDOT:PSS
CNC_3	35% PCN : 5% CNC	60% NGF : 5% CNC	2% CNC : 98% PEDOT:PSS

Preparation of PLA ink

The PLA ink contained the same functional materials as the CNC ink (NGF and PCN). These materials were mixed with the PLA binder, which had to be prepared first. To prepare the PLA binder, PLA pellets were dissolved in Cyrene, obtaining a 10 wt% solution. The solution was stirred magnetically overnight at 80 °C. Once the PLA binder had been prepared, NGF and PCN were added to the PLA dispersion. If needed, to obtain the appropriate concentration of each material, a specific quantity of Cyrene was added to the mixture. Once all the compounds had been added, the dispersion was stirred using a homogenizer at 30 000 rpm for 20 min to obtain the final ink. A scheme of the development of the PLA inks is shown in Fig. 3. PLA-based formulations are shown in Table 4.

Preparation of electrode ink

Electrode ink (hereafter termed "AC ink") was prepared following a method reported earlier.[46]

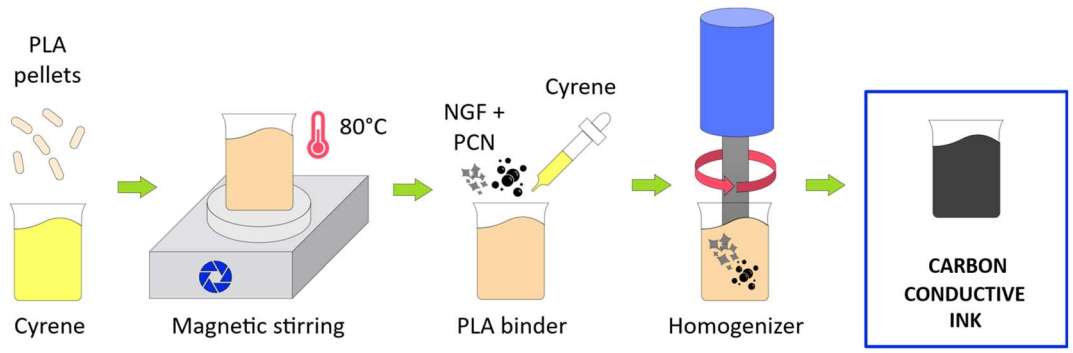

Fig. 3 Ink synthesis process.

Table 4 Formulations of PLA-based inks

	Functional material : binder (wt%)		
Name	PCN : CNC	NGF : CNC	Binder : solvent (wt%)
PLA_1	35% PCN : 50% PLA	15% NGF : 50% PLA	10% PLA : 90% Cyrene
PLA_2	20% PCN : 25% PLA	55% NGF : 25% PLA	10% PLA : 90% Cyrene
PLA_3	25% PCN : 20% PLA	55% NGF : 20% PLA	5% PLA : 95% Cyrene

The chitosan water-based binder was prepared by mixing 1.7 g of chitosan with 67.6 g of water and 0.7 g of acetic acid. The mixture was magnetically stirred overnight. After preparing the chitosan binder, electrode ink was prepared by mixing mechanically 6.89 g of chitosan binder with 3.09 g of activated carbon and 2 g of water.

Synthesis of the reline electrolyte

Reline was prepared by combining choline chloride and urea in a 1 : 2 molar ratio and warming the mixture to 80 °C under continuous stirring (VMS C7 Advanced, VWR) until it turned into a clear, uniform liquid.[35–37] After cooling to room temperature, the resulting mixture was used as the electrolyte for SCs.

Material characterization

Measurement of sheet resistance. A critical parameter for the use of these inks as CC of a capacitor is the measured sheet resistance of an applied layer of 30 μm. Sheet resistance measurements were performed using Four-Point Probe equipment from Ossila. Before measurements, samples were prepared on a rectangular geometry depositing the ink on a PET film using Doctor Blade™ (Fig. 4) and drying the samples in an oven at 60 °C. CNC-based ink samples were dried for 30 min, while PLA-based ink samples were dried for 150 min to ensure solvent evaporation (Fig. S1). As a mask, a 50 μm-thick polyimide film was used. The thickness of the prepared samples was measured using a digital micrometre from Mitutoyo. The obtained sheet resistance of the used HCC ink was 13.8 ± 0.1 Ω sq^{-1}. Table 5 details the measured sheet resistances of the prepared inks. As shown in Table 5, and analysing the relationship between particles and binders provided in Tables 3 and 4, the higher the particle content is in the binder, the lower the sheet resistance obtained.

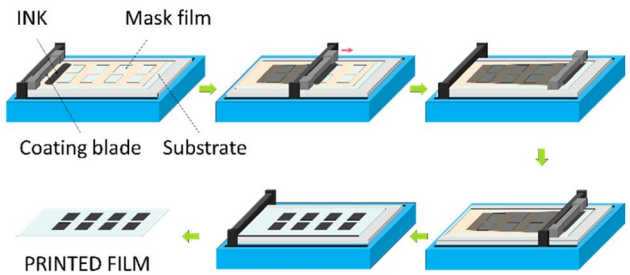

Fig. 4 Deposition scheme using Doctor Blade™.

Table 5 Sheet resistances of inks with different compositions

CNC inks		PLA inks	
Name	Sheet resistance (Ω sq^{-1})	Name	Sheet resistance (Ω sq^{-1})
CNC_1	844 ± 8	PLA_1	19 000 ± 200
CNC_2	17.3 ± 0.1	PLA_2	43.3 ± 0.4
CNC_3	6.2 ± 0.1	PLA_3	11.4 ± 0.1

This behaviour could be explained by the space remaining between the particles when the solvent is evaporated. The greater the particle concentration, the less space between particles and the less binder between them. This leads to a higher contact area, which improves the electrical conductivity of samples and reduces the sheet resistance.

The obtained sheet resistance values could be compared with those in previous studies on the development of sustainable inks based on different materials. For example, Najafi *et al.*[16] reported the development of PLA-based inks with a conductivity of ~55 S m^{-1} for a 0.3 mm-printed layer. Brooke *et al.*[17] studied a cellulose carbon ink and obtained a conductivity of 400 S m^{-1}. We prepared inks with a conductivity of 5.3 × 10^3 S m^{-1} and 2.9 × 10^3 S m^{-1} for CNC_3 and PLA_3 ink, respectively, for a 30 μm ink-applied layer, which were higher conductivity values.

With the obtained results, one ink of each group was selected for use as a CC for the SC. The selected inks were CNC_3 and PLA_3. Nevertheless, when measuring the sheet resistance, the CNC_3 ink started to crack, making it a poor option for use as the CC of SCs (Fig. S2). In this way, only the PLA_3 ink was selected for subsequent experiments. Table 6 shows the final composition of the selected ink. Composition is shown in wt%.

Viscosity measurements. Rheological measurements were performed using the hybrid rheometer Discovery 2 DHR-2 from TA Instruments. Rheological assessment of HCC and PLA inks revealed several details regarding their printability and structural integrity during processing. As depicted in Fig. 5a, the apparent viscosity of PLA and HCC inks demonstrated

Table 6 Final composition of the selected ink

	% functional material				
Name	% PCN	% NGF	% binder (PLA)	% solvent (Cyrene)	Sheet resistance (Ω sq^{-1})
PLA_3	9%	19.5%	7.5%	64.0%	11.4 ± 0.1

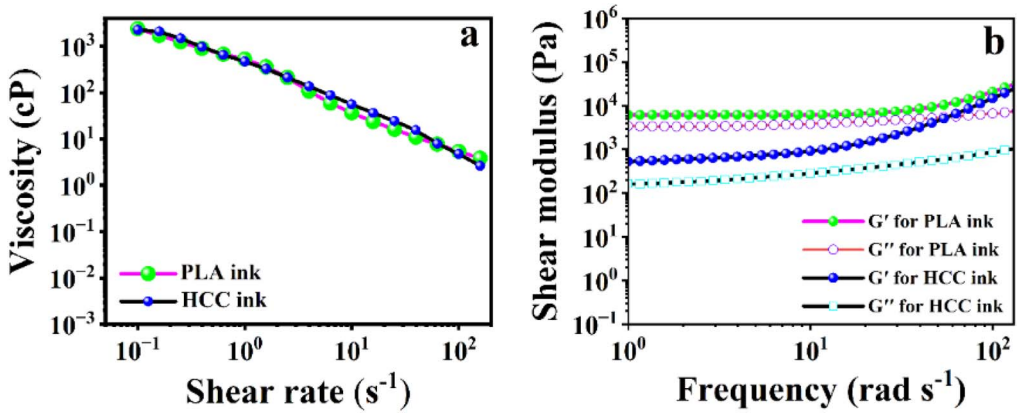

Fig. 5 (a) Variation in the apparent viscosity of both inks with respect to shear rate. (b) Storage modulus (G') and loss modulus (G'') of the inks plotted as functions of angular frequency.

a pronounced decrease with increasing shear rate, indicative of typical shear-thinning behaviour.[47]

This feature is vital for printed electronics because it ensures that inks can be smoothly extruded or deposited at high shear rates while maintaining sufficient viscosity for uniform pattern formation at rest.[48] Additionally, Fig. 5b provides insights into the viscoelastic characteristics of these formulations by plotting the storage modulus (G') and loss modulus (G'') over a range of angular frequencies. For PLA and HCC inks, the storage modulus remained higher than the loss modulus, which implied that the ink behaved more like an elastic solid than a viscous liquid in these conditions.[37,47] This result suggested the inks had the internal strength to keep their shape once printed, resisting deformation over time. It also hinted at a stable microstructure formed during formulation, likely supported by interactions between components such as polymers, fillers, or binders.

Scanning electron microscopy (SEM). SEM was performed on the samples. As shown in Fig. 6, the SCs were composed of two printed layers (CC and electrode), where the electrode was printed on top of the CC layer. For these reasons, two samples were prepared by Doctor Blade™. The inks used and drying conditions are shown in Table 7. SEM was performed on the top of each layer, and a cross-sectional image was also taken. The obtained images are shown in Fig. 6. The Blade-coater layer of PLA_3 ink had a rough surface compared with the HCC ink. This can be seen from Fig. 6a and e, which exhibit higher rugosity at a lower magnification.

Table 7 Inks and drying conditions of the samples prepared for SEM

Sample	HCC ink	PLA ink
CC ink	HCC ink	PLA_3
Drying conditions	30 min at 90 °C	2 h 30 min at 60 °C
Electrode ink	AC ink	AC ink
Drying conditions	30 min at 60 °C	30 min at 60 °C

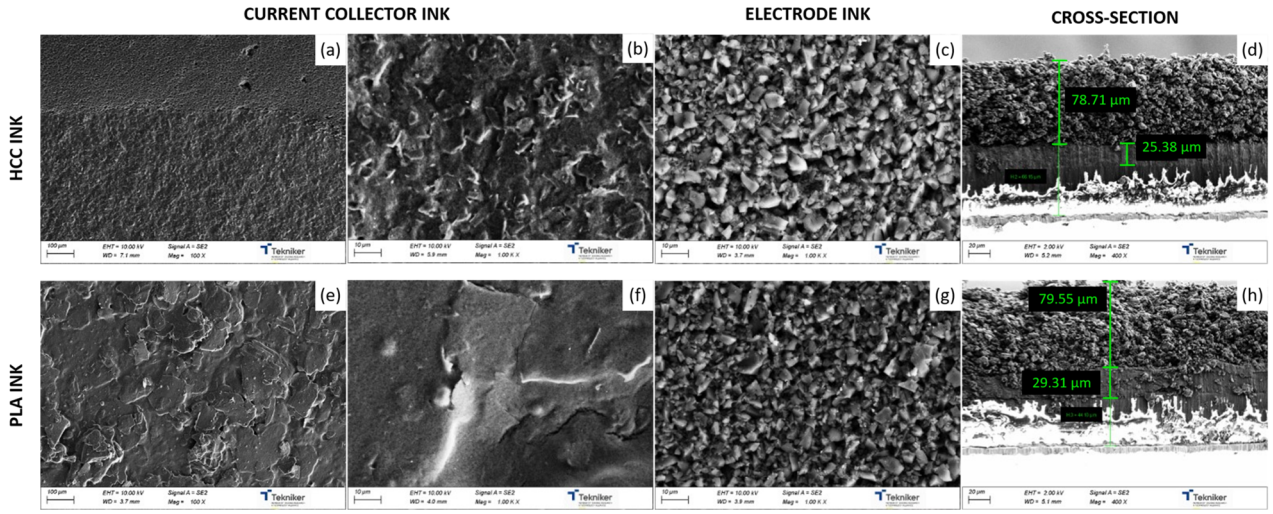

Fig. 6 Scanning electron microscopy. (a) HCC ink (top view; magnification: 100×), (b) HCC ink (top view; magnification: 1000×), (c) electrode ink (top view) printed on HCC ink. (d) Cross-section of HCC ink and electrode ink. (e) PLA ink (top view; magnification: 100×). (f) PLA ink (top view; magnification: 1000×). (g) Electrode ink (top view) printed on PLA ink. (h) Cross-section of PLA ink and electrode ink.

Rugosity was also appreciated upon optical microscope images in Fig. S2. Nevertheless, the cross-sectional image showed good interconnection between the CC layers and the electrode layers.

Fabrication of SCs

Symmetrical SCs were manufactured following consecutive steps as described below and shown in Fig. 7.

(1) Print and dry the CC ink onto the substrate.
(2) Print and dry the electrode ink on top of the CC.
(3) Add the electrolyte to the electrode and let it soak for 1 h.
(4) Place the separator in its position.
(5) Place the sealant in its position.
(6) Assembly of the SC.

Devices were fabricated using two types of CCs: the conductive ink developed in PLA ink and HCC ink. Each ink required its own curing conditions. The HCC ink was cured at 90 °C for 30 min. The PLA-based ink needed a longer and gentler curing step of 2 h and 30 min at 60 °C to ensure appropriate film formation without damaging the polymer. The electrodes were prepared using an activated carbon ink made from chitosan binder, activated carbon, and water as per our previous work.[35–37,42] This ink was designed to maintain good adhesion on the CC while keeping the formulation nontoxic. The coated electrodes were cured at 60 °C for 30 min. Reline was used as the electrolyte, and the electrodes were allowed to soak in it for 1 h before assembly to support ion infiltration and improve the initial performance of the device. A cellulose paper sheet was used as the separator, and PET film was chosen as the substrate. All coatings were applied with a blade coater using a Kapton mask. CCs were coated using a 150 μm blade gap to achieve a uniform conductive layer, while a 50 μm gap was used for the electrode layer to ensure good contact and controlled thickness.

SC characterization

After fabrication, the SC were tested up to 1.8 V at current densities of 0.5 A g^{-1}, 1 A g^{-1}, and 5 A g^{-1} using a Maccor 4300 system. Two samples were selected for extended cycling to study long-term behaviour. For these, electrochemical impedance spectroscopy (EIS) was performed before and after cycling to monitor changes in resistance. EIS measurements were carried out on a Zahner potentiostat across a frequency range of 1 MHz to 100 mHz, using a 5 mV AC signal at open-circuit potential. The cycling protocol on the Maccor system was designed to accelerate ageing. Every 1000th cycle was recorded at 0.5 A g^{-1} to track performance in detail, while the remaining cycles were run at 5 A g^{-1} to accelerate the test. This combination provided a good balance between realistic cycling behaviour and time-efficient evaluation. The specific capacitance and equivalent series resistance (ESR) were determined from galvanostatic charge–discharge (GCD) data using eqn (1) and (2).[49]

$$C_{\text{device}} = \frac{I\mathrm{d}t}{\mathrm{d}V} \quad (1)$$

$$\text{ESR} = \frac{V_{\text{drop}}}{I} \quad (2)$$

Results and discussion

Ink development

Two ink compositions were developed, achieving HCC ink sheet resistance, as shown in Table 8. Nevertheless, CNC inks were not a good option for developing SCs onto a PET substrate due

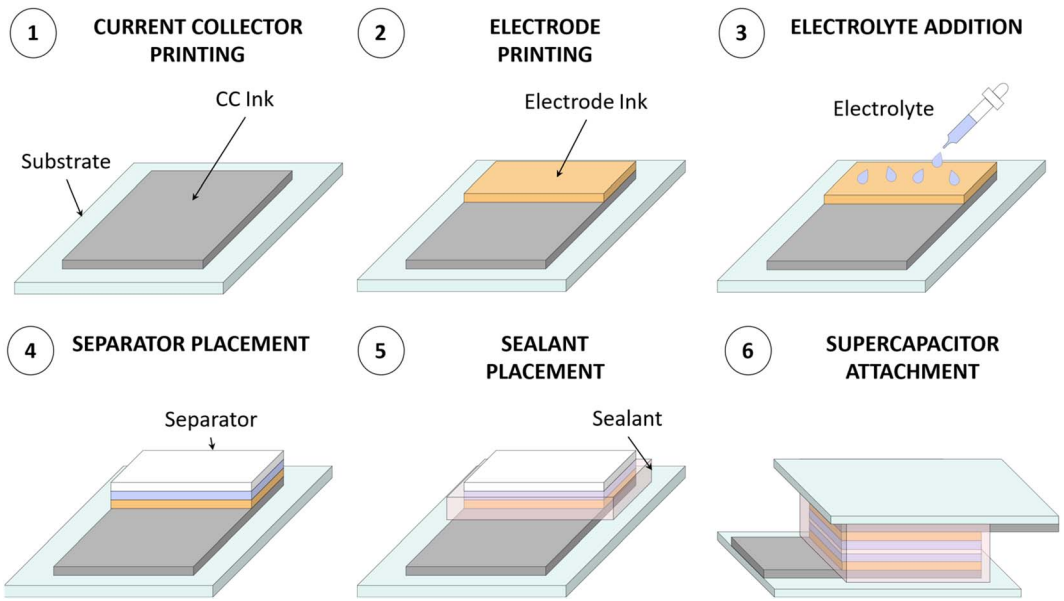

Fig. 7 SC manufacturing. (1) CC printing. (2) Electrode printing. (3) Electrolyte addition. (4) Separator placement. (5) Sealant placement. (6) SC attachment.

Table 8 Sheet resistance of graphite and developed inks

Name	HCC ink	CNC_3	PLA_3
Sheet resistance (Ω sq^{-1})	13.8 ± 0.1	6.2 ± 0.1	11.4 ± 0.1

to poor adhesion and cracking (Fig. S2). Compatibilities using other substrates could be studied.

The PLA-based composition had good adhesion to the PET substrate, becoming a good option to use as a CC to develop SCs.

Electrochemical performance of PLA ink as a CC for SC

To assess the feasibility of the synthesized PLA ink as a CC material, a set of SCs was fabricated, and we compared their performance with devices prepared using HCC under identical conditions.

The electrochemical performance data presented in Fig. 8 summarize the direct comparison. Fig. 8a presents the CV curves measured at a scan rate of 5 mV s^{-1} for devices made with HCC ink and PLA ink. Both devices showed well-defined, box-shaped curves with good symmetry across a window of 0 to 1.8 V. This indicated that each device could operate reliably within this potential range. Closer examination of the CV profiles showed a clear electrochemical performance gap between the two CC inks.

The device fabricated with the PLA ink-based CC exhibited a distinctly higher current density throughout the voltage window compared with the one using the HCC ink. This stronger current response indicated that the PLA ink formulation formed a more efficient current-collecting network, allowing charges to move more freely at the electrode–electrolyte interface. The improved conductivity pathways and better interfacial contact provided by the PLA ink translated directly into enhanced charge storage behaviour. Fig. 8b shows the GCD curves of the HCC device and PLA-based ink device recorded at a current density of 0.5 A g^{-1}.

The PLA ink-based device exhibited a noticeably longer discharge period than the HCC device, clearly indicating its superior capacitive performance. Significantly, the PLA ink-based device reached a higher capacitance of 125 mF at the same current density than that of the HCC ink device (60 mF). SEM revealed that a rougher surface on the PLA ink-based CC increased the electrode mass loading, which explained the increased capacitance compared with samples based on HCC. Despite the clear comparison of electrode loading, the results demonstrated that the PLA ink-based CC lowered the resistance of SC. In addition, the PLA ink-based device and HCC device exhibited comparable rate capability, maintaining >65% of their initial capacitance as the current density increased from 5 A g^{-1}. This consistency indicated that each device could operate reliably under higher charge and discharge rates.

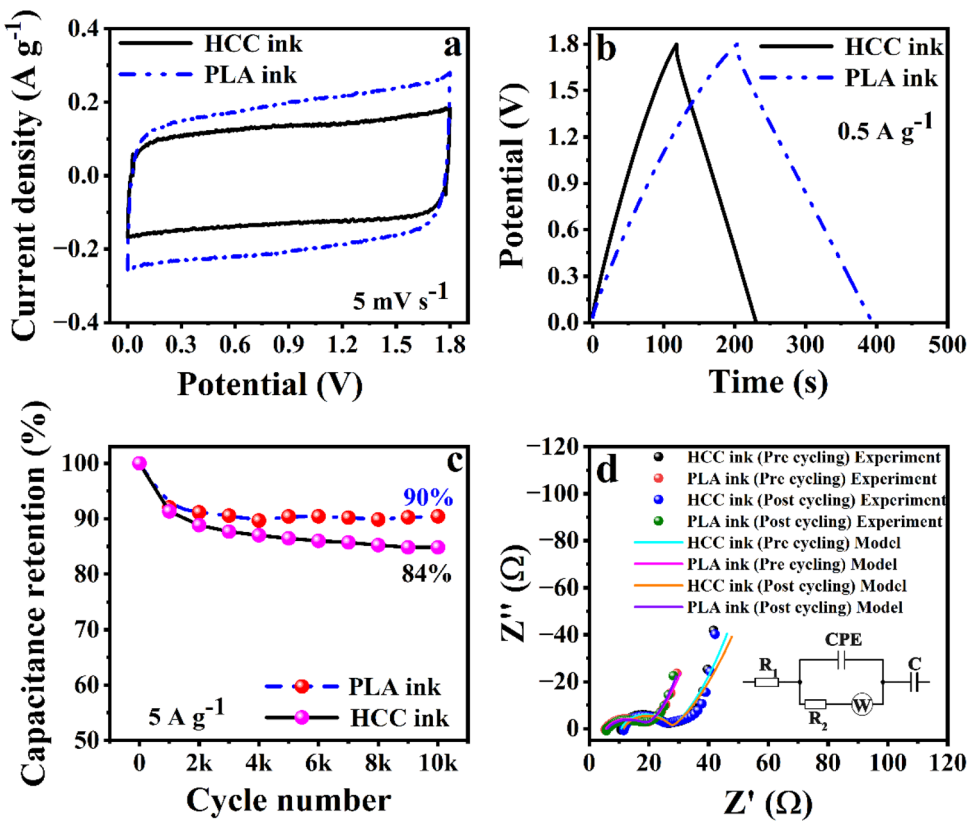

Fig. 8 Differences in CC electrochemical performance through (a) CV curves, (b) GCD profiles, (c) capacitance retention during cycling and (d) Nyquist plots recorded before and after 10 000 cycles (inset shows the equivalent circuit used for fitting and solid lines are the fitting results).

Moreover, the PLA ink-based device demonstrated strong cycling stability, showing only a 10% decrease in capacitance after 10 000 cycles, as shown in Fig. 8c. In comparison, the HCC device retained ~84% of its initial capacitance over the same cycling period. This highlighted the improved long-term durability of the PLA ink-based CC. Coulombic efficiency describes how effectively stored charge can be recovered from an energy storage device or electrode. It is calculated as the ratio of the charge released during discharge to the charge initially stored during the charging process.[50] The high coulombic efficiency observed throughout cycling indicated the excellent charge reversibility and stable electrochemical behaviour of the device (Fig. S3). EIS was employed to gain a deeper understanding of the resistive and capacitive processes governing device operation.

The Nyquist plots displayed in Fig. 8d and the corresponding fitting parameters presented in Table 9 reveal the characteristic features of porous electrode systems. They comprise a high-frequency intercept representing the series resistance (R_s), a depressed semicircle associated with charge-transfer kinetics modelled *via* a constant-phase element (CPE), and a low-frequency tail attributable to diffusive ion transport (Warburg impedance).

R_s accounts for the combined resistance of the electrolyte, electrode conduction pathways, CC sheet resistance, and interfacial contact resistance.[50] The R_s values extracted before cycling were 5.59 Ω for the PLA ink-based device and 10.7 Ω for the HCC ink-based device. The significantly lower R_s of the PLA ink-based device was consistent with the higher intrinsic conductivity of the PLA ink-based printed CC, superior adhesion between the printed electrode and CC that reduces interfacial losses, and lower effective ionic resistance due to improved microstructural porosity and electrolyte accessibility, although these effects are not uniquely proven by EIS alone. After 10 000 cycles, R_s increased only slightly for the PLA ink-based device (5.59 → 6.04 Ω) but more prominently for the HCC ink-based device (10.7 → 11.5 Ω), indicating that the HCC ink CC underwent larger structural or interfacial degradation. In printed SCs, such increases in R_s are typically associated with microcrack formation and delamination. The depressed semicircle in the Nyquist plot represents charge-transfer resistance at the electrode–electrolyte interface. At precycling, R_{CT} was 13.4 Ω for the PLA ink and 16.5 Ω for the HCC ink. A lower R_{CT} indicates good electron exchange at the interface, better electrochemical accessibility of the active material, and a more uniform and stable CC surface. Such associations are consistent with our data, but impedance analysis alone does not prove specific microstructural causes. The PLA ink-based device consistently showed lower R_{CT} due to its more homogeneous printed microstructure and smoother interface that promotes charge-transfer kinetics. After cycling, R_{CT} remained nearly unchanged for the PLA ink-based device (13.4 → 13.3 Ω), whereas the HCC ink-based device showed a slightly decreased but less stable R_{CT} (16.5 → 15.8 Ω). ESR values obtained from GCD measurements are higher than those derived from EIS[25,49] because GCD depicts the total device resistance. In our case, the combined R_s and R_{CT} values from EIS were ~19 Ω for the PLA ink-based device and ~27 Ω for the HCC ink-based device, while the ESR from GCD was ~28 Ω and ~36 Ω, respectively.

The CPE describes non-ideal capacitive behaviour, and is defined by two parameters: Y_0, the pseudo-capacitance expressed in μS s^{α}, and α, a dimensionless phase exponent ranging from 0 to 1. An ideal capacitor exhibits $\alpha = 1$, and any deviation from this value reflects increasingly distributed interfacial processes and time constants; lower α does not uniquely indicate surface roughness because different types of heterogeneity can give similar CPE behaviour.[50] At precycling, the PLA ink-based device showed a substantially higher Y_0 of 551 μS s^{α} with an α of 0.7, consistent with a larger effective electrochemically active area and more heterogeneous interfacial response. In contrast, the HCC ink-based device displayed a much lower Y_0 of 24.1 μS s^{α} and a slightly higher α of 0.79, suggesting a more homogeneous interfacial response but a significantly smaller effective electrochemical area contributing to charge storage. After 10 000 cycles, the PLA ink-based device retained strong capacitive behaviour, with Y_0 nearly doubling, an effect typically associated with improved electrolyte penetration and utilization of the porous structure during cycling. A moderate decrease in α is commonly observed during long-term cycling as the interface undergoes minor restructuring but remains overall stable. In contrast, the HCC ink-based device showed only a modest increase in Y_0. The Warburg diffusion element (W) provides insight into ion transport within the porous electrode, with lower values indicating faster and less hindered diffusion. At precycling, the PLA ink-based device exhibited a lower W of 13.3 DW compared with 21.3 DW for the HCC ink-based device, and after 10 000 cycles, the PLA value decreased slightly to 11.5 DW. In contrast, the HCC device showed an increase in W from 21.3 to 23 DW over the same period. Moreover, the PLA ink-based device showed a very small decrease from 136 to 134 mF, corresponding to only ~1.5% loss, which is consistent with its robust structural integrity and stable ion-storage behaviour. The HCC device exhibited an apparent increase in capacitance from 73.8 to 85 mF after

Table 9 Fitting parameters from equivalent circuit analyses of NaCl-based RAC and PAC devices

		CPE				
Device	R_s (Ω)	Y_0 (μS s^{α})	α	R_{CT} (Ω)	W (DW)	C (mF)
PLA ink precycling	5.59	551	0.71	13.4	13.3	136
PLA ink post cycling	6.04	1080	0.63	13.3	11.5	134
HCC ink precycling	10.7	24.1	0.79	16.5	21.3	73
HCC ink post cycling	11.5	33.6	0.76	15.8	23	85

cycling, but this should not be interpreted as a real improvement in charge-storage performance. These capacitance values were obtained from equivalent circuit modelling of Nyquist plots, and the reliability of the modelled parameters depends strongly on how well the circuit fits the experimental data. Although the selected model fitted R_s, R_{CT}, and the main CPE elements had good accuracy, the fitting accuracy for the Warburg diffusion component and the modelled capacitance in the HCC device deteriorated significantly after cycling, with errors of >30%. This level of uncertainty indicates that the diffusion-dominant region of the HCC impedance spectrum was poorly represented, which artificially inflated the modelled capacitance and created the false appearance of improvement. In contrast, the PLA ink-based device maintained fitting errors of <10% for the same parameters, but even these values were not fully reliable, and, therefore, the capacitance obtained directly from GCD measurements should be considered the true representation of the device behaviour. The deviation in the EIS fit is also clearly visible in Fig. 8d, in which the simulated curve diverges from the experimental data at the tail region of the Nyquist plot. This further confirmed that the modelled capacitance for the HCC device was influenced by fitting limitations rather than real electrochemical enhancement.

For comparison, the biodegradable CC ink reported by Aeby *et al.* (2021) showed electrical conductivities of 260.8 ± 20.1 S m^{-1}, 219.8 ± 21.3 S m^{-1}, and 228.1 ± 22.6 S m^{-1} for measurements taken parallel, perpendicular, and at 45°, respectively, to the printed lines.[51] Given the 27 Ω per square, another useful reference is the edible SC reported by Durukan *et al.* in 2024, in which the carbon-based HGC (hydroxyethylcellulose/glycerol/carbon) electrode acted as both the electrode and CC, yielding a sheet resistance of ~40 Ω per square at 10 μm.[52] Although this design is appropriate for ingestible applications, it has clear drawbacks: the conductivity remains modest, the architecture depends on relatively thick and carbon-rich films, and the lack of a dedicated CC limits device engineering and restricts optimization of individual layers. In contrast, the PLA-based ink developed in this work achieved a sheet resistance of 16 Ω per square at a thickness of only 30 μm, demonstrating a clear improvement in conductivity while using a substantially thinner printed layer. The PLA ink-based SCs exhibited a specific energy of 22 W h kg^{-1} along with a specific power of 0.4 kW kg^{-1} based on the total mass loading of electrode materials. These values are comparatively higher than those of HCC devices, which deliver 13 W h kg^{-1} at the same specific power of 0.4 kW kg^{-1}. For comparison, we selected studies that reported printed SCs fabrication using activated carbon electrodes in symmetric configurations; the corresponding electrochemical data are summarized in Table S1. Also, we performed a simple light-emitting diode (LED) demonstration using the SC fabricated with PLA ink, and the results are included in the SI. Fig. S4 illustrates the connection setup for the LED. Once the circuit was closed, the LED emitted a dim-red light. SC was first charged using a current source up to 1.8 V, after which the voltage was maintained for several minutes to reduce leakage current. The fully charged SC was then connected to the red LED. This demonstration confirmed the effective energy storage and discharge capability of the SC. This improvement highlighted the potential of our formulation to enable thinner, more conductive, and more sustainable CCs for future printed energy storage devices. In future work, we will focus on reducing the sheet resistance further towards values of <10 Ω per square to strengthen the performance and broaden the applicability of these inks.

Sustainability discussion

Development of two sustainable inks for CC was studied: one water-based and another solvent-based. For both inks, natural carbon particles were used as functional materials. As binder materials, biodegradable polymers have been used: cellulose and PLA. Cellulose has been demonstrated to be biodegradable when processed with fungal enzymes or microbes.[53] PLA degrades through hydrolysis in moist environments. Moreover, degradation can be accelerated by adding certain enzymes (*i.e.* proteinase K or bromelain).[54] The solvents we used were PEDOT:PSS aqueous dispersion and Cyrene, which were classified by the supplier as "greener alternative products".[55,56] Moreover, Cyrene is a biomass solvent, does not have known toxicity issues,[57] and European Union research has classified it as a "safe bio-solvent".[58] Considering all the materials used, the developed inks could be considered sustainable for two main reasons: their materials are bio-based or biodegradable.

Considering the electrode ink, the binder we used was chitosan, which is a natural and biodegradable polymer under various conditions (enzymatic pathways, hydrolytic, thermal, oxidative degradation).[59] The solvent is an aqueous dissolution of acetic acid, which has been demonstrated to undergo anaerobic degradation.[60]

Reline electrolyte was prepared by combining choline chloride, which is a safe, non-toxic and biodegradable, and urea, and this combination has been demonstrated to be biodegradable.[61] The separator used in the SC was cellulose paper, which, as with the cellulose used to develop CC ink, is degraded under fungal enzymes or microbes.[53]

Table 10 Composition of the sustainable developed inks and the obtained sheet resistance

	% functional material				
Name	% PCN	% NGF	% binder	% solvent	Sheet resistance (Ω sq^{-1})
CNC_3	10%	17.5%	CNC: 1.5%	PEDOT:PSS: 71%	6.2 ± 0.1
PLA_3	9%	19.5%	PLA: 7.5%	Cyrene: 64.0%	11.4 ± 0.1

Although the PET substrate and barrier were not degradable, the developed SC is a more sustainable option and a step toward greener electronics. The substitution of these materials will be explored in future studies.

Considering material recovery, some strategies should be followed at the end of life of the devices. The first step should be the detachment of the SC structure. Afterwards, the electrolyte and electrode materials were aqueous solutions; strategies such as recovering the materials by dissolving them in water could be followed to reprocess them. Considering PLA ink, a similar strategy using Cyrene as the solvent could be implemented to recover the materials present in the ink (Fig. S4). Other strategies, such as solvothermal recovery, should be analysed to reprocess the used materials.[62] Hence, less material consumption and e-waste will be ensured.

Conclusions

The synthesis of new sustainable conductive inks was studied. Two formulations were created using carbon particles as the functional material. The obtained inks exhibited sheet resistances comparable to those of HCC ink ($13.8 \pm 0.1\ \Omega\ sq^{-1}$). Formulation and sheet resistance values are shown in Table 10. Nevertheless, CNC-based inks cracked upon application to the substrate and drying, so the CNC formulation was discarded for SC applications (Fig. S2).

The inks formulated in this work represent an advance in the development of conductive, sustainable inks. Najafi *et al.*[16] also reported the development of PLA-based and green solvent inks with a maximum conductivity of $\sim$55 S m^{-1} for a 0.3 mm-printed layer. Brooke *et al.*[17] reported a cellulose carbon ink achieving a conductivity of 400 S m^{-1}. Comparing the conductivity obtained in this work, CNC_3 and PLA_3 ink had a conductivity of 5.3×10^3 S m^{-1} and 2.9×10^3 S m^{-1}, respectively, for a 30-micron ink-applied layer.

SCs were fabricated using the PLA ink-based CC ink together with a bio-based activated carbon electrode ink. EIS showed that the PLA ink delivered lower ESR than the HCC ink. Although the PLA ink layers had a rougher surface than the HCC coating, this texture increased the effective contact area between printed layers, which, in turn, enhanced the overall capacitance of the device.

We acknowledge that a fully decoupled analysis of mass loading, surface morphology, and CC properties would require a more systematic study with independently controlled variables. Such an investigation is beyond the scope of the present work, but represents an important direction for future research.

Our primary objective was to demonstrate the feasibility of the developed PLA-based ink as a multifunctional material for printed energy storage devices, using SCs as a representative application. A greener printed SC was developed by using sustainable materials on its printed layers.

Author contributions

Leire Sanchez-Duenas was involved in the conceptualization, data curation, data analyses, investigation, methodology and validation of the developed inks and SCs, and in writing the original draft. Chirag Mevada supported conceptualization, data curation, data analyses and validation of SCs, and writing sections of the original draft. Timo Punkari contributed with the investigation, data analyses and validation of the electrolyte of the SC, and writing sections of the original manuscript. Estibaliz Gómez contributed with SUINK project administration, funding acquisition, providing the needed resources and writing (reviewing and editing) the manuscript. Estibaliz Aranzabe contributed significantly to the design of the methodology, supervising and reviewing and editing the manuscript. Matti Mäntysalo supervised this work and contributed to funding acquisition, as well as reviewing and editing the manuscript. J. L. Vilas-Vilela contributed by supervising the methodology and reviewing the manuscript.

Conflicts of interest

There are no conflicts of interest to declare.

Data availability

Ref. 36, 37, 39, 40, 42–44, 51 and 63–66 are cited in the supplementary information (SI). For any further data requests, please contact the corresponding authors at leire.sanchez@tekniker.es or chirag.mevada@tuni.fi. Supplementary information: drying conditions, optical microscope images, coulombic efficiency, specific energy and power, supercapacitor demostration by lighting a LED and material recovery information. See DOI: https://doi.org/10.1039/d5ta10407f.

Acknowledgements

Our study was supported by the SUINK project funded by the Horizon Europe research and innovation programme of the European Union (101070112). The views and opinions expressed are, however, those of the author(s) only, and do not necessarily reflect those of the European Union or the European Commission. Neither the European Union nor the granting authority can be held responsible for them. Additionally, the research has utilized "Printed Intelligence Infrastructure" provided by the Research Council of Finland, supported by grant number 358618.

Notes and references

1 X. Huang, Y. Liu, S.-W. Hwang, S.-K. Kang, D. Patnaik, J. F. Cortes and J. A. Rogers, *Adv. Mater.*, 2014, **26**, 7371–7377.
2 L. Sanchez-Duenas, E. Gomez, M. Larrañaga, M. Blanco, A. M. Goitandia, E. Aranzabe and J. L. Vilas-Vilela, *Materials*, 2023, **16**, 3940.
3 N. Ibrahim, J. O. Akindoyo and M. Mariatti, *J. Sci.: Adv. Mater. Devices*, 2022, **7**, 100395.
4 A. Poulin, X. Aeby, G. Siqueira and G. Nyström, *Sci. Rep.*, 2021, **11**, 23784.
5 L. Sanchez-Duenas, C. Monteserin, E. Gómez, M. Blanco, M. Larrañaga, E. Aranzabe, M. Criado-Gonzalez, R. Rai and

J. L. Vilas-Vilela, in *2024 IEEE International Conference on Flexible and Printable Sensors and Systems (FLEPS)*, 2024, pp. 1–4.
6 Y. Z. N. Htwe and M. Mariatti, *J. Taiwan Inst. Chem. Eng.*, 2021, **125**, 402–412.
7 European Commission and Directorate-General for Environment, *Communication from the Commission to the European Parliament, the Council, the European Economic and Social Committee and the Committee of the Regions EU Policy Framework on Biobased, Biodegradable and Compostable Plastics*, 2022.
8 ISO 14855-2, https://www.iso.org/standard/72046.html, accessed 28 November 2025.
9 ISO 14852, https://www.iso.org/standard/72051.html, accessed 28 November 2025.
10 S. Bonardd, E. Robles, I. Barandiaran, C. Saldías, Á. Leiva and G. Kortaberria, *Carbohydr. Polym.*, 2018, **199**, 20–30.
11 F. Hoeng, A. Denneulin and J. Bras, *Nanoscale*, 2016, **8**, 13131–13154.
12 S. Tuukkanen, J. Toriseva, A. Pammo, J. Virtanen and J. Lahti, in *2020 IEEE 8th Electronics System-Integration Technology Conference (ESTC)*, IEEE, Tønsberg, Vestfold, Norway, 2020, pp. 1–3.
13 E. Chiellini, A. Corti, S. D'Antone and R. Solaro, *Prog. Polym. Sci.*, 2003, **28**, 963–1014.
14 N. A. Stini, P. L. Gkizis and C. G. Kokotos, *Green Chem.*, 2022, **24**, 6435–6449.
15 K. Pan, Y. Fan, T. Leng, J. Li, Z. Xin, J. Zhang, L. Hao, J. Gallop, K. S. Novoselov and Z. Hu, *Nat. Commun.*, 2018, **9**, 5197.
16 M. Najafi, M. Zahid, L. Ceseracciu, M. Safarpour, A. Athanassiou and I. S. Bayer, *J. Mater. Res. Technol.*, 2022, **18**, 5197–5211.
17 R. Brooke, A. Fall, M. Borràs, D. B. Yilma, J. Edberg, S. Martinez-Crespiera, C. Aulin and V. Beni, *Flexible Printed Electron.*, 2021, **6**, 045011.
18 D. Zappi, G. Varani, E. Cozzoni, I. Iatsunskyi, S. Laschi and M. T. Giardi, *Nanomaterials*, 2021, **11**, 3428.
19 J. R. Camargo, T. A. Silva, G. A. Rivas and B. C. Janegitz, *Electrochim. Acta*, 2022, **409**, 139968.
20 Y.-Z. Zhang, Y. Wang, T. Cheng, L.-Q. Yao, X. Li, W.-Y. Lai and W. Huang, *Chem. Soc. Rev.*, 2019, **48**, 3229–3264.
21 T. M. Kraft, M. Kujala, A. Railanmaa, S. Lehtimäki, T. Kololuoma, J. Keskinen, D. Lupo and M. Mantvsalo, in *2018 IEEE 18th International Conference on Nanotechnology (IEEE-NANO)*, 2018, pp. 1–4.
22 B. Tawiah, E. Kofi Howard and B. Asinyo, *BEST: IJMITE*, 2019, **4**(5), 61–78.
23 *Handbook of Print Media*, ed. H. Kipphan, Springer, Berlin, Heidelberg, 2001.
24 D. Yang and A. Laforgue, *J. Electrochem. Soc.*, 2019, **166**, A2503–A2512.
25 C. Mevada and M. Mukhopadhyay, *Ind. Eng. Chem. Res.*, 2021, **60**, 1096–1111.
26 Y. Huang, Y. Li, Q. Gong, G. Zhao, P. Zheng, J. Bai, J. Gan, M. Zhao, Y. Shao, D. Wang, L. Liu, G. Zou, D. Zhuang, J. Liang, H. Zhu and C. Nan, *ACS Appl. Mater. Interfaces*, 2018, **10**, 16572–16580.
27 S. Xie, S. Liu, F. Cheng and X. Lu, *ChemElectroChem*, 2018, **5**, 571–582.
28 G. Wang, H. Wang, X. Lu, Y. Ling, M. Yu, T. Zhai, Y. Tong and Y. Li, *Adv. Mater.*, 2014, **26**, 2676–2682.
29 C. Mevada and M. Mukhopadhyay, *Mater. Chem. Phys.*, 2020, **245**, 122784.
30 M. S. Samuel, C. Mevada and M. Mukhopadhyay, *Arabian J. Sci. Eng.*, 2022, **47**, 5949–5958.
31 M. Liu, J. Liu, Y. Zhang, X. Han, H. Li, Z. Huang and T. Ma, *ChemElectroChem*, 2025, **12**, e202400513.
32 J. Liang, C. Jiang and W. Wu, *Appl. Phys. Rev.*, 2021, **8**, 021319.
33 J. Liang and W. Wu, *Appl. Phys. Rev.*, 2024, **11**, 011301.
34 X. Zhang, C. Jiang, J. Liang and W. Wu, *J. Mater. Chem. A*, 2021, **9**, 8099–8128.
35 C. Mevada, J. Tissari, V. S. Parihar, A. Tewari, J. Keskinen and M. Mäntysalo, *J. Power Sources*, 2024, **624**, 235529.
36 C. Mevada, A. Kattainen, V. S. Parihar, J. Keskinen and M. Mäntysalo, *J. Power Sources*, 2025, **652**, 237596.
37 A. Kattainen, C. Mevada, T. Punkari, V. S. Parihar, H. Pourkheirollah, J. Keskinen and M. Mäntysalo, *J. Power Sources*, 2026, **661**, 238663.
38 C. Mevada, J. Tissari, V. S. Parihar, A. Tewari, J. Keskinen, M. Kellomäki and M. Mäntysalo, *J. Mater. Chem. A*, 2024, **12**, 24357–24369.
39 C. Mevada, V. S. Parihar, A. Tewari, J. Keskinen, M. Kellomäki and M. Mäntysalo, *IEEE Journal on Flexible Electronics*, 2025, **4**, 42–51.
40 C. Mevada, A. Kattainen, V. S. Parihar, A. Tewari, J. Keskinen and M. Mäntysalo, in *2025 IEEE International Conference on Flexible and Printable Sensors and Systems (FLEPS)*, IEEE, Singapore, 2025, pp. 1–4.
41 J. Keskinen, A. Railanmaa and D. Lupo, *J. Energy Storage*, 2018, **16**, 243–249.
42 T. Punkari, J. Keskinen, A. Kattainen, J. Laakso, M. Honkanen and M. Mäntysalo, *J. Power Sources*, 2024, **621**, 235301.
43 K. M. Adam, C. Mevada, V. S. Parihar, A. Tewari, H. Pourkheirollah, J. Keskinen and M. Mäntysalo, *Biomass Bioenergy*, 2026, **208**, 108857.
44 C. Mevada, A. Kattainen, V. S. Parihar, A. Tewari, J. Keskinen, M. Kellomäki and M. Mäntysalo, *J. Mater. Chem. A*, 2026, **14**, 4759–4775.
45 *T68 Synthetic Graphite Sheet – T-Global Technology – Products*, https://www.tglobaltechnology.com/product/t68-synthetic-graphite-sheet/, accessed 28 October 2025.
46 C. Mevada, J. Tissari, V. S. Parihar, A. Tewari, J. Keskinen and M. Mäntysalo, *J. Power Sources*, 2024, **624**, 235529.
47 F. Zeng, X. Song, J. Liang, X. Zhang, X. Sha, X. Wu, H. Zhou, Z. Liu, W. Wu and C. Jiang, *J. Mater. Chem. A*, 2022, **10**, 25148–25158.
48 S.-Z. Guo, M.-C. Heuzey and D. Therriault, *Langmuir*, 2014, **30**, 1142–1150.
49 S. Zhang and N. Pan, *Adv. Energy Mater.*, 2015, **5**, 1401401.

50 A. Noori, M. F. El-Kady, M. S. Rahmanifar, R. B. Kaner and M. F. Mousavi, *Chem. Soc. Rev.*, 2019, **48**, 1272–1341.
51 X. Aeby, A. Poulin, G. Siqueira, M. K. Hausmann and G. Nyström, *Adv. Mater.*, 2021, **33**, 2101328.
52 M. B. Durukan, D. Keskin, Y. Tufan, O. Dincer, M. O. Cicek, B. Yildiz, S. Çınar Aygün, B. Ercan and H. E. Unalan, *Adv. Funct. Mater.*, 2024, **34**, 2307051.
53 J. Li, Y. Long, F. Yang and X. Wang, *Curr. Opin. Solid State Mater. Sci.*, 2020, **24**, 100806.
54 S. Shrestha, M. Snowdon and D. B. Levin, *Polymers*, 2025, **17**, 3042.
55 PEDOT:PSS, https://www.sigmaaldrich.com/ES/es/product/aldrich/483095, accessed 8 January 2026.
56 Cyrene, https://www.sigmaaldrich.com/ES/es/product/sial/807796, accessed 8 January 2026.
57 F. P. Byrne, S. Jin, G. Paggiola, T. H. M. Petchey, J. H. Clark, T. J. Farmer, A. J. Hunt, C. Robert McElroy and J. Sherwood, *Sustainable Chem. Processes*, 2016, **4**, 7.
58 *Presentación de dos nuevos biodisolventes no tóxicos para los procesos de captura de carbono*, https://cordis.europa.eu/article/id/446811-introducing-two-new-non-toxic-bio-solvents-for-carbon-capture-processes/es, accessed 26 January 2026.
59 I. Koumentakou, A. Meretoudi, C. Emmanouil and G. Z. Kyzas, *J. Ind. Eng. Chem.*, 2025, **146**, 70–86.
60 *H. F. Program, Environmental Decisions*, https://www.fda.gov/food/food-ingredients-packaging/environmental-decisions, accessed 27 January 2026.
61 K. Radošević, M. Cvjetko Bubalo, V. Gaurina Srček, D. Grgas, T. Landeka Dragičević and I. Radojčić Redovniković, *Ecotoxicol. Environ. Saf.*, 2015, **112**, 46–53.
62 J. Zhou, X. Zhou, W. Yu, Z. Shang, Y. Yang and S. Xu, *Nano Energy*, 2024, **120**, 109145.
63 S. Azmi, M. F. Koudahi and E. Frackowiak, *Energy Environ. Sci.*, 2022, **15**, 1156–1171.
64 Z. J. Zhang, G. L. Deng, X. Huang, X. Wang, J. M. Xue and X. Y. Chen, *Electrochim. Acta*, 2020, **339**, 135940.
65 H. Pourkheirollah, R. I. M. Vitto, A. Volperts, S. T. Vindt, L. Grīnberga, G. Kučinskis, J. Keskinen and M. Mäntysalo, *Carbon Trends*, 2025, **18**, 100436.
66 R. I. M. Vitto, H. Pourkheirollah, A. Volperts, S. T. Vindt, L. Grīnberga, G. Kučinskis, C. Mevada, J. Keskinen and M. Mäntysalo, in *2025 IEEE International Conference on Flexible and Printable Sensors and Systems (FLEPS)*, IEEE, Singapore, 2025, pp. 1–4.